Journal of Nanoporous Systems

Original Research Paper

Design of a Nanoporous Magnetic Nanocomposite Based on Montmorillonite Nanoneedles and Humic Acid for Dye Adsorption: RSM Optimization, Kinetic, Thermodynamic, and Isotherm Studies

Zahra Abbasi[1], Abdolhadi Farrokhnia[2], Elisa Isabel Garcia-Lopez[3], Zahra Zohrabzadeh[4], Ermia Aghaie[5], Yashar Behnamian[6]

[1] *Department of Chemistry, Faculty of Basic Sciences, Ayatollah Boroujerdi University, Boroujerd, Iran*
[2] *Department of Chemistry, Faculty of Science, Shahid Chamran University of Ahvaz, Ahvaz, Iran*
[3] *''Schiavello-Grillone'' Photocatalysis Group, Dipartimento di Energia, Ingegneria dell'informazione e Modelli Matematici (DEIM), Universita` di Palermo, Viale delle Scienze, 90128 Palermo, Italy*
[4] *Department of Physics, Faculty of Science, Shahid Chamran University of Ahvaz, Ahvaz, Iran*
[5] *School of Engineering, University of British Columbia - Okanagan, Kelowna, Canada*
[6] *Department of Chemical and Materials Engineering, University of Alberta, Canada*

Article history
Received: 4 November 2025
Revised: 19 November 2025
Accepted: 23 December 2025

*Corresponding author
Zahra Abbasi, Department of Chemistry, Faculty of Basic Sciences, Ayatollah Boroujerdi University, Boroujerd, Iran.
Email: Z.Abbasi@abru.ac.ir

Abstract: This study investigates low-cost, reusable Fe_3O_4@Humic acid/montmorillonite core-shell nanocomposites as high-efficiency adsorbents for removing methyl orange (MO) dye from aqueous solutions. The nanocomposites were characterized using FT-IR, TEM, SEM, XRD, and BET/BJH analysis to assess structural and surface properties. The results showed a specific surface area (30.23 m^2/g), a total pore volume (0.098 cm^3/g), and average pore diameter (in the mesoporous range of 1-10 nm) for the Fe_3O_4@HA/MMT composite. Adsorption efficiency was optimized over 300 minutes using response surface methodology (RSM) with a five-factor, three-level central composite design. Kinetic studies revealed that the process follows a pseudo-second-order model ($R^2 > 0.99$). Equilibrium data were evaluated using Langmuir, Freundlich, Temkin, Dubinin–Radushkevich, and Harkins–Jura isotherms, with the Freundlich model providing the best fit, indicating multilayer adsorption on a heterogeneous surface. Thermodynamic analysis showed: That negative $\Delta G°$ values confirm spontaneity, while their magnitudes (-6.26–-9.86 kJ/mol) suggest physical adsorption. The positive $\Delta H°$ value (19.31 kJ/mol) confirms that the process is endothermic. Increased entropy (88.84 J/mol·K) points to enhanced surface disorder and MO-adsorbent interactions. The positive activation energy (E_a = 18.3 kJ/mol) further corroborates the endothermic nature. A near-zero sticking probability ($S^* \approx 10^{-5}$) reinforces the physical adsorption mechanism. These findings highlight the nanocomposite's potential as a sustainable, high-performance solution for dye wastewater treatment.

Keywords: Core-Shell structure; Reusable adsorbent; Standard enthalpy; Kinetic; Mathematical modeling.

Introduction

Textile manufacturing contributes to the economies of numerous countries globally. This process generates wastewater with varying colors, depending on the extent of dye fixation on the substrates, which is influenced by the nature of the chemicals, the intended colour intensity, and the treatment procedure [1]. The substantial volumes of wastewater generated by dye-manufacturing and dye-utilizing enterprises pose significant environmental hazards. The global output of dyes and pigments is estimated to reach at 800,000 tons annually, with a minimum of 10% released into the environment. Recent years have seen the investigation of many strategies for the removal of pollutants in wastewater, including adsorption [2, 3], biodegradation [4, 5], photocatalysis [6,

7], and biocatalytic oxidation [8, 9]. Among them, adsorption has been the generally utilized and effective approach in wastewater treatment. Surface adsorption occurs in both physical and chemical forms. Physical adsorption, driven by van der Waals forces between pollutant molecules and the adsorbent surface, is one of the most common types of adsorptions and has reversible properties. On the other hand, chemical adsorption occurs due to a chemical reaction between the pollutant and the adsorbent surface. This adsorption type has a low velocity and is irreversible, unlike physical adsorption [1]. Various adsorbents have been studied for the removal of organic dyes and contaminants. The use of cheap and eco-friendly adsorbents increases the value of the adsorption operation. Numerous types of adsorbents have been utilized to remove the dye in wastewater. The application of Fe_3O_4 nanoparticles (NPs) as highly efficient adsorbents has attracted significant interest due to advantages such as relatively low cost, large specific surface area, and high adsorption capacity. In this study, a magnetic adsorbent was synthesized using inexpensive, natural materials, and the methyl orange dye adsorption kinetics was investigated. As a coating agent, different weight percentages of humic acid were added to iron oxide, and the weight percentage of sodium montmorillonite to the synthesized adsorbent structure was investigated. Different methods were employed to characterize the synthesized samples. Afterward, the synthesized adsorbent has been used by considering five parameters and examining the effect of these parameters on the maximum efficiency of methyl orange dye removal, using Design-Expert software. The software results indicated the optimal percentages of sodium montmorillonite (MMT) and humic acid (HA) for synthesizing the adsorbent. Ultimately, under these optimal conditions, the kinetics and thermodynamics of the adsorption process were examined.

Materials and Methods

$FeCl_3.6H_2O$, $FeCl_2.4H_2O$, NH_3, Humic acid ($C_{187}H_{186}O_{89}N_9S_1$), NaOH, and HCl were purchased from Merck, Germany. NaCl and methyl orange ($C_{14}H_{14}N_3NaO_3$) were bought from Sigma Company. Sodium montmorillonite (Cloisite Na^+ with a cation exchange capacity (CEC) of 92.6 mequiv. 100 g clay was supplied by Nanocor Inc. All reagents were of analytical grade and used as received without further purification.

Preparation of Fe_3O_4@HA/MMT

To synthesize the Fe_3O_4@HA composite, 1:2 ratio of $FeCl_3.6H_2O$ and $FeCl_2.4H_2O$ dissolved in 50 ml of distilled water in a three-neck round-bottom flask connected with a reflux condenser and with magnetic stirring was stirred to provide a homogeneous solution until the temperature reached 80 °C. At this temperature, 10% humic acid (HA) (30 and 50 wt% for another ratio) was added to this mixture under constant stirring. After this time, 50 mL of 25% ammonium hydroxide was added to this mixture under constant stirring and kept at 80 ℃ for an additional 120 min. The synthesized Fe_3O_4@HA composites were separated by a magnet and washed with distilled water several times. Finally, a powder product was collected and dried at 80 °C for 8 h. To prepare Fe_3O_4@HA/MMT, 1.8 g of the Fe_3O_4@HA composite was dispersed in 100 mL of ethanol under ultrasound for 40 min separate dishes, 450 mg MMT (94.7 and 257 mg for another ratio) were dispersed in 20 mL water under ultrasound for 60 min. Then, MMT and Fe_3O_4@HA solutions were added slowly. The mixture was mechanically stirred at room temperature for 24 h. The product Fe_3O_4@HA/MMT was obtained by washing with water and ethanol. Finally, the sample was dried at 80 ℃ overnight [2, 3].

Investigation of Adsorbent Activity on Removal of Methyl Orange Solution

The methyl orange dye solution was used to investigate the laboratory efficiency of the synthesized adsorbent. The experimental design and number of runs were determined using Design Expert software and the CCD method. In this research, five independent parameters were used that include adsorbent content (1-5 $g.L^{-1}$), pH (3-9), the humic acid weight percentage (10%-50%), sodium montmorillonite weight percentage (5%-20%), and the initial concentration of methyl orange dye solution (5-25 $mg.\ L^{-1}$). Each of these five independent parameters was determined in high- and low-level values, considering the α= 1.

Adsorption Experiments

We have used response surface methodology (RSM) to model the relationship between the quantitative factors and the response and to detect optimal factors that display the "best" response. These designs can fit a second-order prediction equation for the response as follows:

$$R = \beta_0 + \sum_{i=1}^{k} \beta_i X_i + \sum_{i=1}^{k} \beta_{ii} X_i^2 + \sum_{i=1}^{k} \sum_{j=1}^{k} \beta_{ij} X_i X_j + e_0 \quad (1)$$

Here, R is the predicted response (% Removal); X_i and X_j are variables; β_0 is the constant coefficient; Also, β_i is a factor that defines the effect of parameter ion the final response. The β_{ij} is the cross-product coefficient, and β_{ii} is the quadratic coefficient, which returns to the effects of the interaction among independent variables. The coefficient can be derived using multiple regression analysis, and the equation can be utilized to forecast the response. The parameter values can be ascertained using Eq. 2.

$$x_i = \frac{X_i - X_0}{\delta X} \quad (2)$$

Here, X_0 is the real value of the independent variable at the center point, xi is the real value of the independent

variable, and δX is the step change value between low (-2) and high (+2) levels. The percentage removal of color was calculated using Eq. 3:

$$\text{Percentage Removal (\%)} = \frac{(C_0 - C_f)}{C_0} \times 100 \quad (3)$$

Where, C_0 is the initial concentration of dye and C_f is the final concentration of dye after adsorption.

Kinetics of adsorption was determined by analyzing the adsorbent sorption of the dye from an aqueous solution at different time intervals. To identify adsorption isotherms, dye solution at different temperatures (25–55 ˚C) with known amounts of adsorbents was shaken until the equilibrium was achieved. To compare the adsorptive capacity and intensity of different adsorbents, batch tests were performed. The equilibrium adsorption capacity was calculated from Eq. 4.

$$q_e = \frac{(C_0 - C_e)V}{W} \quad (4)$$

Where q_e (mg. g^{-1}) is the equilibrium adsorption capacity, C_e is the dye concentration at equilibrium, V (L) is the volume of solution, and W (g) is the weight of adsorbent.

Results and Discussion

Characterization

The morphologies of all synthesized samples were determined by scanning electron microscopy (SEM) and transmission electron microscopy (TEM) methods. The crystal phases of the samples were analyzed using an X-ray Diffraction (XRD) analysis with radiation (λ = 0.15418 nm). A scan rate of 0.11 s^{-1} was applied to record the powder XRD patterns for 2θ in the range of 10–70°. The Fourier transform infrared (FT-IR) spectra of the as-synthesized material were taken at room temperature using a 100 mg KBr pellet containing 1 mg of the sample. The adsorption measurement was taken by UV–UV-Visible spectrophotometer (Cintra 101 GBC Scientific Equipment Ltd.). Brunauer–Emmett–Teller method was used to calculate the specific surface area from the adsorption isotherms.

XRD diffraction patterns of Fe_3O_4@HA (50%) and Fe_3O_4@HA(50%)/MMT-Na(12.5%) samples were shown in Figure 1.

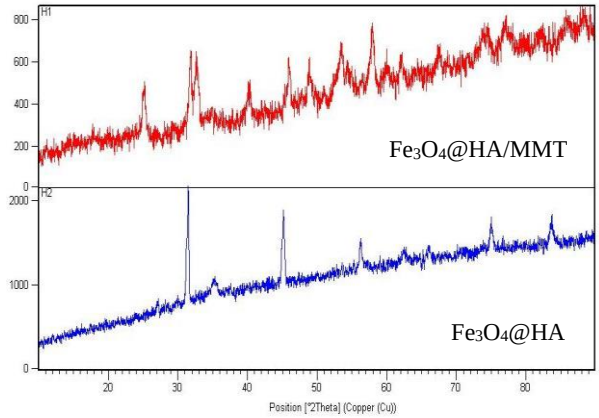

Fig. 1. XRD patterns for the nanocomposites.

The peaks that appeared at 2θ = 57.8, 43.2, 35.6, and 30.2 are related to iron oxide. The peaks that appeared at 2θ = 27.8, 35.1, 62.5, 68.1, and 74.2 are attributed to the sodium montmorillonite structure. The presence of peaks in both iron oxide and sodium montmorillonite structures in the XRD pattern of nanocomposites indicates that a successful crystalline structure and dispersion of sodium montmorillonite with Fe_3O_4@HA core-shell structure [2, 3].

The surface morphology of the nanocomposites was evaluated using the SEM method. Figure 2-a reveals the SEM images of the nanocomposites. A core-shell structure was found that was related to Fe_3O_4 surrounded by HA. Also, in Figure 2-b, the surface structure of Fe_3O_4@HA core-shell composites with sodium montmorillonite were detected.

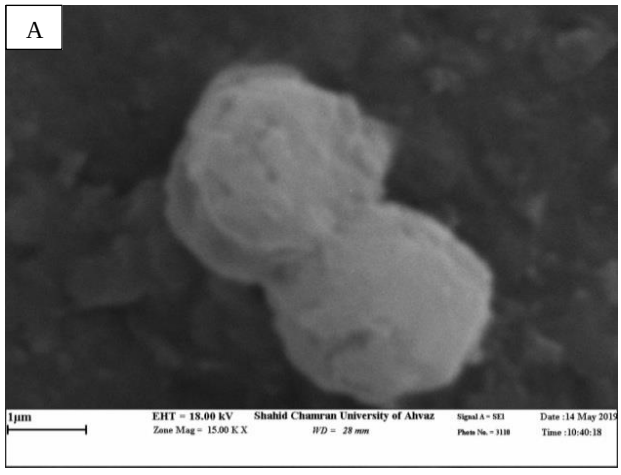

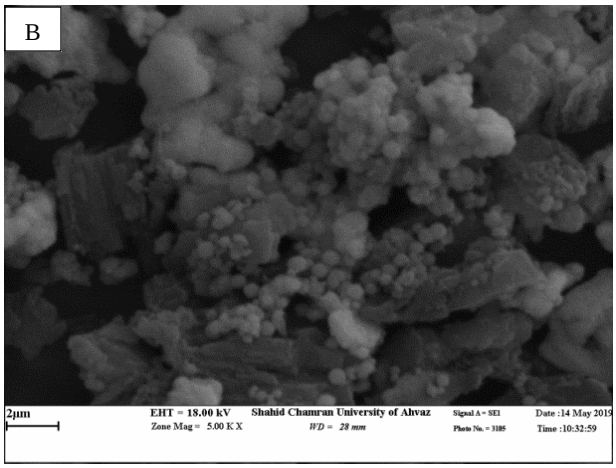

Fig. 2. SEM micrographs of the (A) Fe_3O_4@HA, (B) Fe_3O_4@HA/MMT

TEM images of the synthesized adsorbent are demonstrated in Figure 3. That indicated the core-shell structure of Fe_3O_4@HA. Also, dispersion of the montmorillonite structure was observed alongside the core-shell structure.

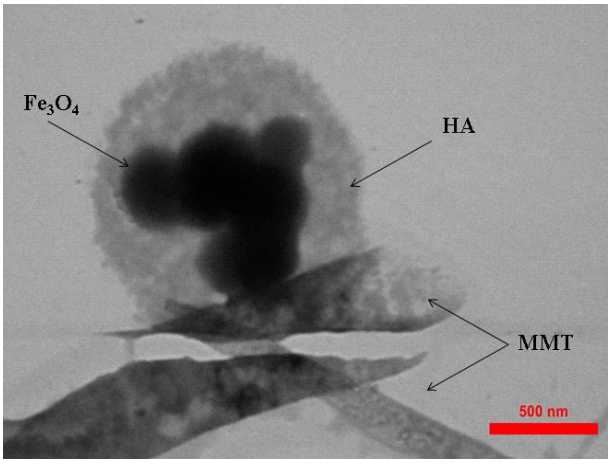

Fig. 3. TEM images of the Fe_3O_4/HA/MMT nanocomposite

The spectra obtained from the Fourier transform infrared analysis are shown in Figure 4. A peak could be seen at 3445 cm^{-1} in the sodium montmorillonite FTIR spectra, which was related to the vibration of the attracted OH in the silicate layer. The peaks around 674 and 449 cm^{-1} were attributed to vibration-attraction of O-Al and vibration-bending of O-Si, respectively. The absorption at 1030 cm^{-1} was linked to the vibration attraction of the O-Si silicate layer. Also, the presence of absorption around 890 and 1052 cm^{-1} was assigned to the vibration of MMT hydroxylans consisting of Al_2OH and MgAlOH. The OH group at 3450 and 1600 cm^{-1} in humic acid spectra was detected clearly. Also, a carbonyl C=O vibration bond at 1680 cm^{-1} was observed. In the Fe_3O_4@HA spectra, the peak at 560 cm^{-1} indicates the Fe-O vibration bond. As observed from synthesized Fe_3O_4@HA/MMT composite spectra, it was found that there were two peaks at 584 and 440 cm^{-1}, which could be attributed to Fe-O vibration attraction bonds, Al-O vibration attraction, and O-Si vibration bending, which means the formation of the synthesized adsorbent. A COO-Fe bond was also observed at 1591 and 1395 cm^{-1} [2, 3].

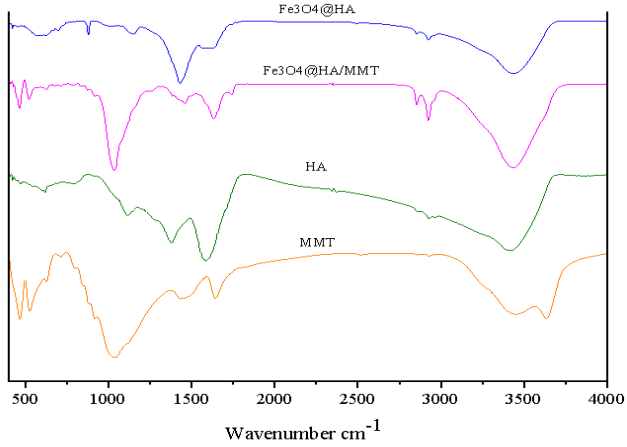

Fig. 4. FT-IR spectra for the nanocomposites.

The BET method is one of the most popular techniques to determine the porous structure of solids, along with other methods like BJH, t-plot, and S_a, which are used to characterize pore distribution. These methods provide general information about adsorption behavior, the shape of the adsorption isotherm, and the average pore size [3, 4]. Figure 5 shows the adsorption-desorption curve of nitrogen gas at a constant temperature on the surface of Fe_3O_4@HA/MMT.

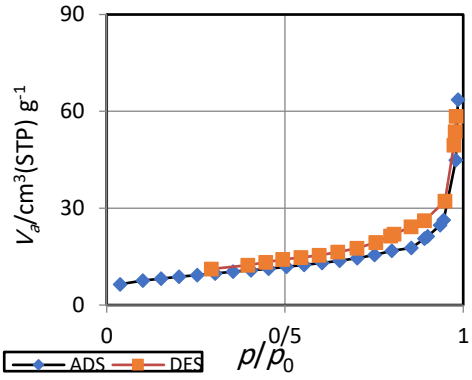

Fig. 5. The adsorption-desorption curve of Fe_3O_4@HA/MMT.

According to IUPAC classification, the samples follow IV type isotherm, which illustrates the presence of material with meso pore's structure. Using BET analysis data, specific surface area for Fe_3O_4@HA/MMT was obtained 30.23 m^2. g^{-1}. In the Fe_3O_4@HA, several iron oxide particles created a core and were surrounded by humic acid as a shell. The spherical core-shell structure of Fe_3O_4@HA with MMT has a higher specific surface area

than the Fe_3O_4@HA structure. The general volume of pores for Fe_3O_4@HA/MMT was obtained at 0.098. Comparing the results of BET analysis and the surface area of the synthesized photocatalyst agrees with the results of previous reports in this field. The distribution of the size of the pores that was calculated using the BJH method and the surface desorption curve is shown in Figure 6. It can be seen that the size of pore diameter for Fe_3O_4@ HA/MMT is in the range of 1-10 nm, which confirms the theory of mesopores [3].

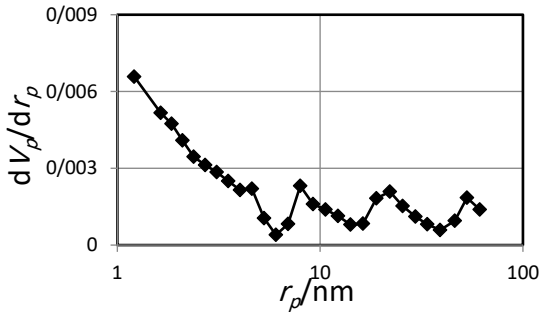

Fig. 6. The distribution of the size of the pores.

The pH of dye solutions has a critical effect on adsorption processes, notably on the adsorption capacity. Its importance is due to the surface charge of the adsorbent, the degree of ionization of the chemicals in the solution, and the separation of the functional groups in the adsorbent sites.

According to Figure 7, pH_{pzc} was calculated at 4.55. At pH values less than pH_{pzc}, the adsorbent surface has a positive charge, and at pH values more than pH_{pzc}, the adsorbent surface has a negative charge. The adsorption rate was changed depending on whether the substance was cationic or anionic, and its interaction with the positive or negative adsorbent surface.

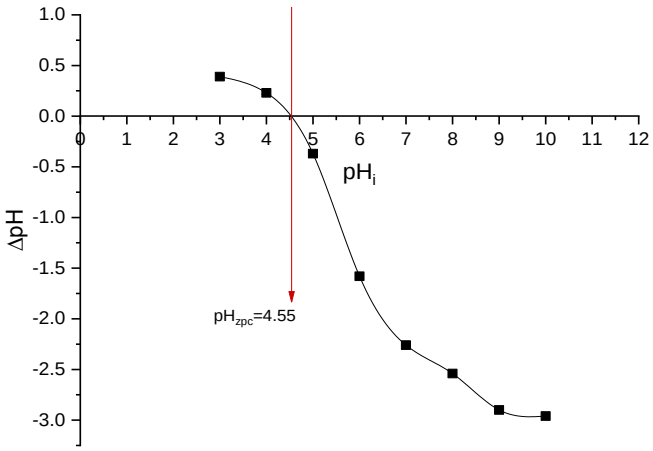

Fig. 7. pH_{pzc} the Fe_3O_4@HA/MMT

This experiment covers the adsorption of methyl orange dye, an anionic chemical. Therefore, at pH values **above** the point of zero charge (pHpzc), adsorption is unfavorable due to electrostatic repulsion between the anionic dye molecules and the negatively charged adsorbent surface [14, 15]. In alkaline pH circumstances, the concentration of hydroxyl groups in the environment rises, resulting in a negative surface charge on the adsorbent. Consequently, a feeble connection or even a repulsive force between the absorbed substance and the adsorbent surface will be established, reducing the adsorption rate.

Results

In this research, design expert software was used to investigate the effect of five parameters on methyl orange dye removal using Fe_3O_4@HA/MMT adsorbents. The design of the experiment was performed using the response surface method using the CCD model. Each independent parameter was examined at five levels in the central compound model. In this study, the value of $\alpha = 1$ was considered. The methyl orange dye removal percentage in the determined experiments was calculated using Eq. 3.

Analysis of Variance (ANOVA)

The ANOVA method was used to statistically determine the main effects and essential interactions. The parameters such as mean squared, a sum of squares, the parameter p-value, and the ratio F were calculated. Table 1 reveals the analysis of variance of the quadratic model. According to Table 1, the following can be considered:

Table 1. ANOVA results of the response surface quadratic model for MO removal (%).

ANOVA for Response Surface Quadratic model						
Analysis of variance table [Partial sum of squares - Type III]						
Source	Sum of Squares	df	Mean Square	F Value	p-value Prob > F	

Model	4569.90	20	228.49	16.90	< 0.0001	significant
A-HA	683.11	1	683.11	50.52	< 0.0001	
B-MMT	149.94	1	149.94	11.09	0.0024	
C-pH	2148.88	1	2148.88	158.91	< 0.0001	
D-amount of adsorbent	255.48	1	255.48	18.89	0.0002	
E- initial of concentration	29.74	1	29.74	2.20	0.1488	
AB	22.61	1	22.61	1.67	0.2062	
AC	71.10	1	71.10	5.26	0.0293	
AD	66.99	1	66.99	4.95	0.0340	
AE	73.51	1	73.51	5.44	0.0269	
BC	8.51	1	8.51	0.63	0.4341	
BD	15.54	1	15.54	1.15	0.2925	
BE	60.23	1	60.23	4.45	0.0436	
CD	1.16	1	1.16	0.086	0.7714	
CE	503.24	1	503.24	37.22	< 0.0001	
DE	7.813E-003	1	7.813E-003	5.777E-004	0.9810	
A^2	4.669E-003	1	4.669E-003	3.453E-004	0.9853	
B^2	81.96	1	81.96	6.06	0.0200	
C^2	355.77	1	355.77	26.31	< 0.0001	
D^2	126.68	1	126.68	9.37	0.0047	
E^2	11.36	1	11.36	0.84	0.3669	
Residual	392.15	29	13.52			
Lack of Fit	326.87	22	14.86	1.59	0.2721	not significant
Pure Error	65.28	7	9.33			
Cor Total	4962.05	49				

The p-value of <0.0001 shows that the model is significant, and there is 99.99% assurance that it can be used to predict the optimal response of the removal over the Fe_3O_4@HA/MMT nanocomposite. The Model F-value of 15.36 indicates that the model is significant. Due to the noise, there is only a 0.01% chance that an F-value this large could occur. The "Prob > F" values less than 0.05 demonstrate that model terms are considerable. In this case, A, B, C, D, AC, AD, AE, CE, C^2, D^2 are significant model terms.

R %= +63.39+ 4.48*A+ 2.1*B- 7.95*C+ 2.74*D- 0.7*E+ 0.84*AB 1.49*AC+ 1.45*AD+ 1.52*AE+ 0.52*BC- 0.7*BD+ 1.37*BE- 0.19*CD+ 3.97*CE+ 0.016*DE+ 0.93*A^2- 4.87*B^2+ 12.88*C^2- 0.97*E^2 (5)

Table 2 presents the effective value of each parameter, its standard errors, regression coefficients, and standard effect values. If the values of the parameters are written according to actual values, Equation 9 is obtained:

$$R\% = +108.80673 - 0.057990 * MMT - 21.24692 * pH + 104.55757 * amount\ of\ adsorbent - 1.02932 * intitial\ of\ concentration + 5.60417E - 003 * HA * MMT - 0.024844 * HA * pH + 0.36172 * HA * amount\ of\ adsorbent + 7.57813E - 003 * HA * intitial\ of\ concentration + 0.022917 * MMT * pH - 0.46458 * MMT * amount\ of\ adsorbent + 0.018292 * MMT * intital\ of\ concentration - 0.31771 * pH * amount\ of\ adsorbent + 0.13219 * pH * intital\ of\ concentration + 7.81250E - 003 * amount\ of\ adsorbent * intital\ of\ concentration + 2.31552E - 003 * HA^2 - 0.086645 * MMT^2 + 1.43069 * pH^2 - 156.84483 * amount\ of\ adsorbent^2 - 9.73793E - 003 * intital\ of\ concentration^2 \quad (6)$$

Concerning the values given in Table 2 and the values of the P ratios, it can be concluded that the proposed model can be considered statistically significant.

Table 2. Model summary statistics.

Source	Std. Dev.	R-Squared	Adjusted R-Squared	Predicted R-Squared	PRESS	
Linear	6.21	0.6584	0.6196	0.5461	2252.43	
2FI	5.06	0.8243	0.7467	0.6420	1776.56	
Quadratic	3.68	0.9210	0.8665	0.7345	1317.55	Suggested
Cubic	3.57	0.9640	0.8740	-0.0425	5175.86	Aliased

Design of Response Surface Experiment

One of the most powerful designs is the complete factorial RSM approach. The CCD technology was chosen to generate surface data because the optimization studies based on the response surface approach are the Equation for this technique. The response surface of the proposed linear model was implemented, and five different components were evaluated. Each element was set at five levels. The five primary and critical parameters are pH (3-9), amount of adsorbent (1-5 g/l), w/w% HA (10-50%), w/w% MMT (5-20%), and the concentration of dye (5-25 ppm). The 3D and 2D contour plots are graphical representations of the interaction of various elements within certain ranges. Figure 8 illustrates the response surface plot as a function of %HA vs. pH.

The effect of %HA and pH is the same and very significant. The dye degradation increased by increasing the %HA and decreasing the pH. Maximum dye degradation percentage was obtained using maximum %HA (50%) and pH 3. Figure 9 depicts the response surface plot as a function of % HA vs. adsorbent amount. The effect of % HA is greater than the amount of adsorbent. By increasing the %HA dye degradation increased. Figure 10 describes the response surface plot as a function of % HA vs. dye concentration. The effect of % HA on the decolorization is more substantial than the effect of concentration. Degradation of dye molecules increased by grew up the HA%. The most dye degradation percentage was achieved by a maximum amount of %HA (50%). Figure 11 reveals the 3D and 2D response surface generated to show the effect of pH and dye concentration on the COD reduction. By surging the pH of the solution, COD reduction decreased, and the maximum response occurred at pH 3 and 15 ppm concentration of dye solution. By raising pH from 3 to 4, a dramatic increase in COD reduction was observed, whereas, under these conditions, maximum decolorization was observed at pH 3 [5].

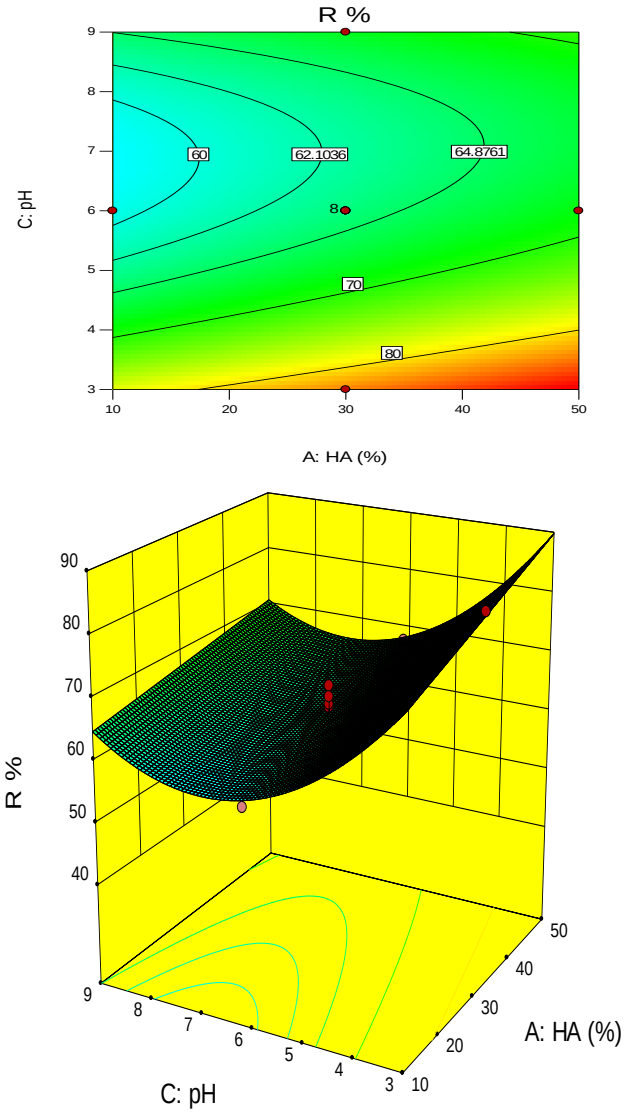

Fig. 8. Interaction effect of %HA and pH on removal of MO.

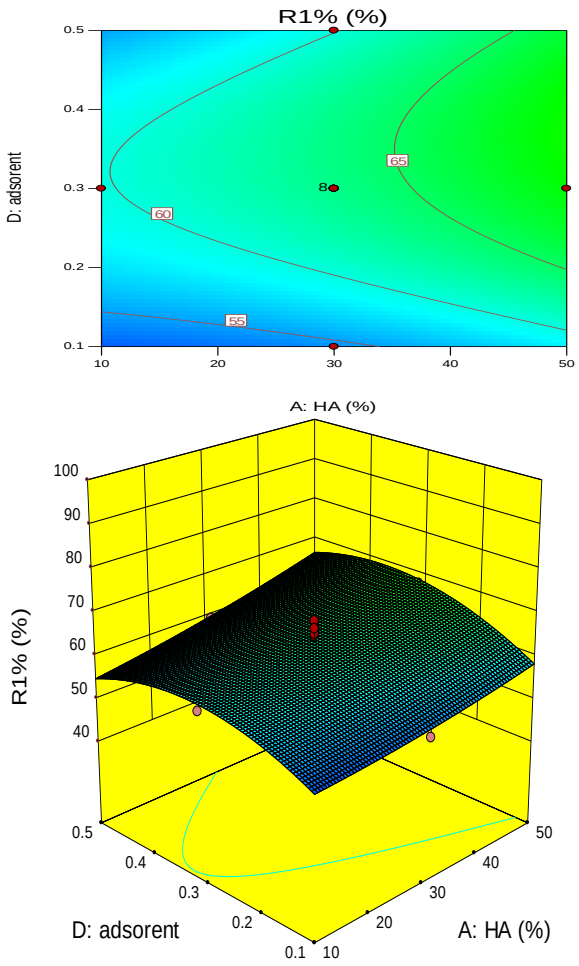

Fig. 9. Interaction effect of %HA and adsorbent on the removal of MO.

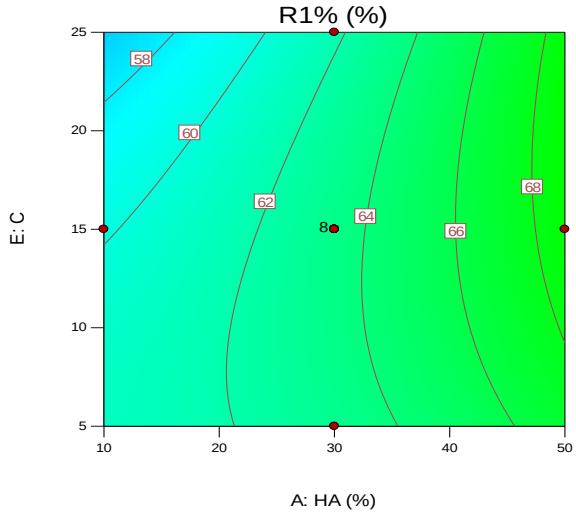

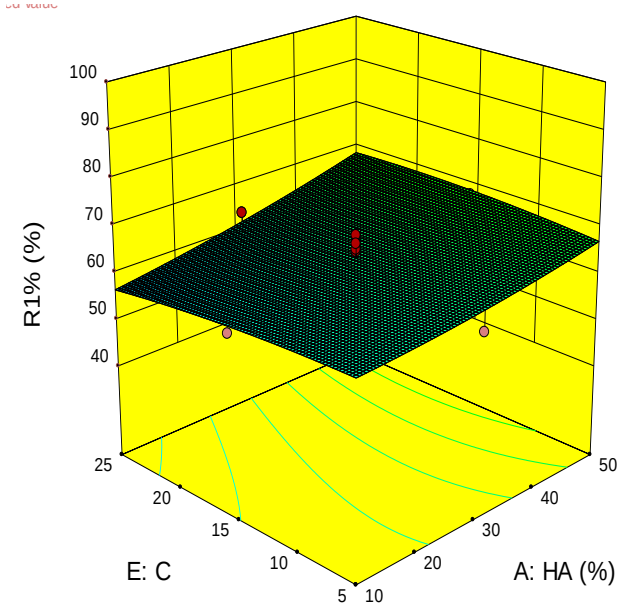

Fig. 10. Interaction effect of %HA and concentration of MO.

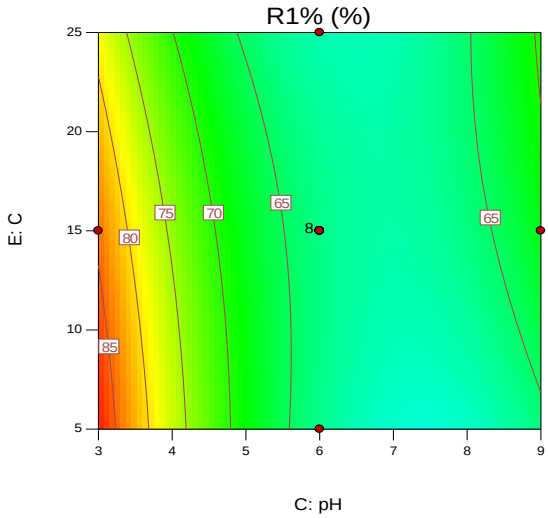

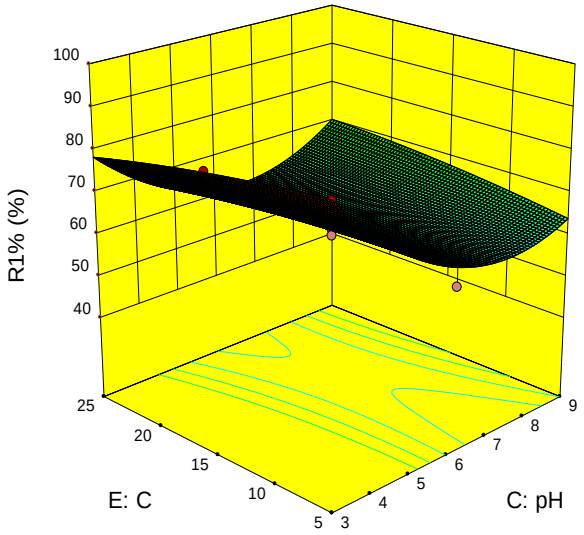

Fig. 11. Interaction effect of concentration of MO and pH on removal of MO.

Optimum Conditions

After the model was established to fit, the optimization purpose of the Design-Expert software was applied to identify the optimal values of the independent variables to create the largest elimination of dye. For each parameter, the top and lower limits of the operating ranges were imposed as a limitation to attain the optimum values. Using the optimization function of the Design-Expert software, the highest removal (96.011%) was predicted under the following conditions: pH 3, %MMT 13.16, %HA 50.00, initial concentration of 5.00 ppm, and an adsorbent dosage of 3.58 g L^{-1}. The predicted optimal removal (96.0%) was experimentally validated, confirming the model's excellent predictive capability.

Kinetic Models

The adsorption of the solid/solution interface is a phenomenon with often complex kinetics. To study the adsorption processes of MO on the adsorbents, pseudo-first-order (PFO), pseudo-second-order (PSO), modified pseudo-first-order (MPFO), modified pseudo-second-order (MPSO), modified pseudo-first-order-2 (MPFO-2), modified pseudo-second-order-2 (MPSO-2), Elovich and intra-particle diffusion kinetic models were studied (Table 3).

Table 3. The kinetic models

Model	Equation	Liner	Initial time
pseudo first order (PFO)	$\frac{dq}{dt} = k(q_e - q)$	$\ln\left(1 - \frac{q}{q_e}\right) = -kt$	$q = kt$
modified pseudo-first-order (MPFO)	$\frac{dq}{dt} = k(\frac{q_e}{q})(q_e - q)$	$\frac{q}{q_e} + \ln(q_e - q) = \ln q_e - kt$	$q = k't^{1/2}$
modified pseudo-first- order-2 (MPFO-2)	$\frac{dq}{dt} = k(\frac{q_e^2}{q^2})(q_e - q)$	$\ln(1 - \frac{q}{q_e}) + \left(\frac{q^2}{2q_e^2}\right) + \frac{q}{q_e} = -kt$	$q = k't^{1/3}$
pseudo-second-order (PSO)	$\frac{dq}{dt} = k(q_e - q)^2$	$\frac{t}{q} = \frac{1}{kq_e^2} + \frac{t}{q_e}$	$q = kt$
modified pseudo-second-order (MPSO)	$\frac{dq}{dt} = k(\frac{q_e}{q})(q_e - q)^2$	$\frac{q}{(q_e - q)} + \ln(1 - \frac{q}{q_e}) = ktq_e$	$q = k't^{1/2}$
modified pseudo-second-order-2 (MPSO-2)	$\frac{dq}{dt} = k(\frac{q_e^2}{q^2})(q_e - q)^2$	$\frac{q}{q_e} + 2\ln(1 - \frac{q}{q_e}) + \frac{q_e}{(q_e - q)} - 1 = ktq_e$	$q = k't^{1/3}$
Elovich	$\frac{dq_t}{dt} = \alpha e^{-\beta q_e}$	$q_t = \frac{1}{\beta}\ln(\alpha\beta) + \frac{1}{\beta}\ln t$	α

The PFO model is the oldest and simplest equation, in which the adsorption rate is expressed in terms of the adsorption capacity [6]. A new correction equation, the first-order Equation for surface adsorption kinetics, has been reported, named the modified pseudo-first-order equation (MPFO) [7]. To improve the kinetic models, Azizian [8] added a new term to the kinetic Equation of the first order and created a new model named modified pseudo-first-order Equation 2 (MPFO-2). In 1999 [9], the pseudo-second-order (PSO) kinetic equation was introduced. The formulation of the PSO model equation is expressed in Table 4. Azizian, by adding a new term to the kinetic Equation of the second-order, produces a new model named modified pseudo-second-order Equation (MPSO). To modify the kinetic models, a new term was added to the kinetic Equation of the order by Azizian and creating a novel model titled modified pseudosecond-order equation-2 (MPSO-2). Another kinetic equation for chemical adsorption was proposed by Elovich recently [10]. This Equation has been used to describe the process of absorbing pollutants from aqueous solutions. Intra-particle diffusion is one of the diffusion-based kinetic models used to describe multistage and competitive adsorptions. This model is used to describe the adsorption process, in which the amount of adsorption depends on the velocity of the adsorbent. The diffusion process of particles into the adsorbent is not confined to one phase. The diffusion rate is high at first, and the particles diffuse into the large pores, then it slows down, and eventually the particles diffuse into the smaller pores. The first process is the migration of methyl orange dye molecules from the aqueous mass to the adsorbent surface through mass diffusion. The second stage is the transmission of colored pollutant molecules from the surface to the adsorbent interior pores, which occurs by intraparticle diffusion. The third step is to absorb the species on the material's surface with a chemical reaction by changing the ionization, complexing, and Chelating [11]. Finally, the second-order kinetic model demonstrated the highest correlation coefficient. It can be claimed that the kinetic reaction is of the second-order kinetic kind. Also, by sketching a schematic of models, the parameters of the models are determined, as indicated in Table 4.

Table 4. Parameters of the kinetic models.

Kinetic model	k	(mg. g^{-1})q_e	R^2	R^2_{Adj}	Pearson's r
pseudo-first-order (PFO)	0.01171	1.0544	0.987	0.984	-0.994
pseudo-second-order (PSO)	0.01144	1.566	0.997	0.996	0.998
modified pseudo first order (MPFO)	0.00859	1.5617	0.990	0.987	-0.995
modified pseudo second order (MPSO)	0.02821	-	0.932	0.919	0.966
modified pseudo first order-2 (MPFO-2)	0.0048	-	0.966	0.960	-0.983
modified pseudo second order-2 (MPSO-2)	0.03146	-	0.974	0.969	0.987
Elovich equation	(mg.g^{-1}.min^{-1})α	(g.mg^{-1})β	R^2	R^2_{Adj}	Pearson's r
	0.0241	1.862	0.991	0.990	0.996
Intra-particle diffusion	k_{id}	c_i	R^2	R^2_{Adj}	Pearson's r
1	0.10172	1.57	0.999	0.997	0.999
2	0.04111	0.63827	0.932	0.866	0.966
3	0.03865	0.67863	0.989	0.977	0.994

Study of Adsorption Isotherms

The study of surface adsorption isotherms is of particular importance in designing an adsorption system. The shape of an isotherm provides information about the affinity of adsorbate molecules for the adsorbent surface. To optimize the design of a surface adsorption system, a high correlation coefficient of the studied isotherms is essential. To obtain the adsorption capacity of Fe_3O_4@HA (50%)/MMT-Na (16.13%), MO dye equilibrium adsorption isotherms on the adsorbent were investigated using five isotherm models: Langmuir, Freundlich, Temkin, Dubinin-Radushkevich (D-R), and Harkins-Jura (H-J). The experiments for isotherm testing were performed as follows: 0.3585 g of Fe_3O_4/HA (50%)/MMT-Na (16.13%) adsorbent was added to 100 mL of MO dye solution with a specified concentration (3, 5, 8, 10, 15 and 20 mg/L). Using an incubator, the sample was stirred at a constant temperature of 25 °C at 180 rpm. Samples were picked up after 300 minutes to achieve equilibrium concentration. After separating the adsorbent using a spectrophotometric device, the absorbance of the solution was checked at a wavelength of 464 nm (maximum wavelength of MO). The equilibrium adsorption capacity was calculated.

The Langmuir isotherm is based on the following assumptions: Adsorption is monolayer, the adsorbent surface is perfectly homogeneous and has a limited number of identical sites, and there is very little interaction between neighbouring absorbed molecules. Eq. 7 is the mathematical form of the Langmuir equation in solution:

$$\frac{C_e}{q_e} = \frac{1}{k_L Q_m} + \frac{C_e}{Q_m} \quad (7)$$

Table 6. The parameters of the Freundlich isotherm.

k_F (mg. g^{-1})	$1/n$	R^2	R^2_{Adj}	Pearson's r
3.924	0.781	0.998	0.998	0.999

Where k_L is Langmuir adsorption constant in L.mg^{-1}, Q_m is the maximum capacity of adsorption or single-layer capacity of adsorption in mg. g^{-1}. The parameter of Langmuir isotherm is shown in Table 5.

Table 5. The parameter of Langmuir isotherm.

k_L (L.mg^{-1})	(mg. g^{-1})Q_m	R^2	R^2_{Adj}	Pearson's r
0.5044	11.906	0.95446	0.94308	0.97697

In the Langmuir isotherm, R^2=0.954, and the predicted R^2 was obtained as 0.943. These data are closely related. The Pearson correlation value was 0.977. The maximum adsorption capacity (Q_m) from the Langmuir isotherm is 11.906 mg/g. The value of k_L, was equal to 0.504. Q_m value was largely due to the abundance of adsorption sites in the unit of mass and caused a large number of ions to be absorbed on its surface, while the connection of these ions to the surface can be weak and cause a reduction in k_L.

In the Freundlich isotherm process, the adsorption is assumed to be heterogeneous. This heterogeneous adsorption can be due to differences in the absorbed or adsorbent surfaces [12]. Eq. 8 and 9 express the mathematical and linear form of the Freundlich equation for absorbing liquid on a solid surface, respectively.

$$q_e = k_F C_e^{1/n} \quad (8)$$

$$Log q_e = Log k_F + \left(\frac{1}{n}\right) Log C_e \quad (9)$$

Where k_F is the Freundlich constant, which is the value of the multilayer adsorption capacity of the adsorbent. 1/n is a constant related to adsorption intensity or heterogeneous surface, that named the heterogeneous factor. The parameters of the Freundlich isotherm are shown in Table 6.

In the Freundlich isotherm, R^2=0.998 and equal to predicted R^2 were obtained. The Pearson correlation value was 0.999. The value of 1/n provides information about surface heterogeneity. So, the surface is more heterogeneous if 1/n is closer to zero. Here, the value of 1/n is in the range of 0.2 to 0.8. Therefore, the synthesized adsorbent is a promising adsorbent for removing MO dye. The Temkin isotherm is defined as Eq. 10 [13]:

$$q_e = \frac{RT}{b}\ln(k_T C_e) \quad (10)$$

If, $B = \frac{RT}{b}$, the linear form of the Equation is defined as Eq. 11:

$$q_e = BLnk_T + BLnC_e \quad (11)$$

Where k_T is the Temkin constant, which depends on the maximum bonding energy. R is the global constant of gas (8.314), T is the absolute temperature in terms of Kelvin, and b is the free energy of the network, which depends on the sidelong interactions between the absorbed particles. Due to the interaction of the absorbed molecules with each other, the adsorbent is covered in a linear layer. This coverage has reduced the heat adsorption of the molecules. The Temkin isothermal parameters of obedience are shown in Table 7. In the Temkin isotherm, R^2=0.939 and predicted R^2 were obtained 0.924, which are close to each other. The Pearson correlation value was obtained 0.969.

Table 7. The Temkin isothermal parameters

k_T (L.mg^{-1})	$b(kJ.mol^{-1})$	R^2	R^2_{Adj}	Pearson's r
9.075	1.379	0.939	0.924٩	0.969

In the Dubinin-Radushkevich (D-R) isotherm, the hypothesis that the surface is homogeneous is not considered. The D-R model is explained by Eq. 12 [14].

$$q_e = q_m e^{-\beta\varepsilon^2} \quad (12)$$

Where q_e is the concentration of absorbed ions on adsorbent in equilibrium condition in terms of mg. g^{-1}, q_m is theoretical saturation capacity, β is D-R constant that is related to the average free energy of adsorption in terms of mol^2.kJ$^{-2,}$ and ε is the Polanyi adsorption potential, which defines as follow: the amount of energy required to separate an absorbed molecule from the surface of its absorbing position. The linear type of the D-R isothermal is expressed in Eq. 13.

$$\ln q_e = \ln q_m - \beta\varepsilon^2 \quad (13)$$

That ε was obtained using Eq. 14.

$$\varepsilon = RT\ln\left(1+\frac{1}{C_e}\right) \quad (14)$$

Where R is the global constant of gas, T is the temperature in Kelvin, and Ce is the equilibrium absorbed concentrate. The average of free energy adsorption was obtained using Eq. 15.

$$E = \frac{1}{\sqrt{2\beta}} \quad (15)$$

From the average energy adsorption value, physical and chemical adsorption were obtained. The parameters of D-R are illustrated in Table 8.

Table 8. The isothermal parameters of D-R.

β(mol^2.k	q_m(mg.g	E(kJ. mol^{-1})	R^2	R^2_{Adj}	Pearson's r
0.0668	4.49	2.736	0.932	0.914	-0.965

In the D-R isotherm, R^2 equals 0.932, and the predicted R^2 is 0.914. The Pearson correlation value is -0.965. In the D-R isotherm, if the amount of adsorption energy is less than 8 kJ.mol^{-1}, the adsorption is physical due to the weak forces of the van der Waals. If it was in the range of 8-16 kJ.mol $^{-1}$, the adsorption was done by an ion exchange mechanism, and when the energy was between 20-40 kJ.mol $^{-1}$, the adsorption was of a chemical type [15]. Table 8 reveals that the energy adsorption is 2.736 kJ.mol $^{-1}$, which indicates the physical adsorption of methyl orange on the adsorbent surface of Fe_3O_4@HA/MMT.

Harkins-Jura isotherm (H-J) specifies the quantity of multilayer adsorption and the presence of heterogeneous pores at the surface of adsorbents, which are introduced in Eq. 16.

$$\frac{1}{{q_e}^2} = \left(\frac{B}{A}\right) - \left(\frac{1}{A}\right) LogC_e \quad (16)$$

Where, A and B are constant. In the H-J isotherm, R^2 equals 0.782, and the predicted R^2 is 0.727. Pearson's correlation value was -0.884.

In the present study, five widely used isotherms were used to investigate the appropriate isotherm model. Langmuir, Freundlich, Temkin, D-R and H-J models were examined. As can be seen from the diagrams, R^2 of Langmuir, Freundlich, Temkin, D-R, and H-J isotherms are equal to 0.954, 0.998, 0.939, 0.932, and 0.782, respectively. Due to the coefficient R^2, the adsorption of methyl orange on the adsorbent followed the Freundlich isotherm.

Thermodynamic Study

Thermodynamic parameters are one of the principles which have particular importance in characterizing the adsorption process. Determination of thermodynamic characteristics in all adsorption methods is crucial to determine the desirability of the adsorption process. By studying variations in the rate of adsorption (in terms of temperature), it is possible to discover the reaction's nature, whether it was exothermic or endothermic. The ideal temperature was established by evaluating the impact of temperature on achieving maximum adsorption. Also, it could be found that adsorption happens as a chemical or physical bond. To investigate the effect of temperature on MO dye adsorption on synthesized Fe_3O_4@HA (50%)/MMT-Na (13.16%), thermodynamic parameters were examined to confirm the nature of adsorption of this research. The thermodynamic constants, variation in free energy, enthalpy, and entropy were calculated to evaluate the process's thermodynamic

possibility and the spontaneous nature. The experiments related to the calculation of thermodynamic parameters were performed as follows: 0.3585 g of Fe_3O_4@HA (50%)/MMT-Na (13.16%) was added to 100 mL of a 5 mg/L solution of MO dye and stirred for 300 min at 25, 35, 45 and 55°C temperature in a shaker incubator at 180 rpm. The thermodynamic parameters required for adsorption, such as Gibbs free energy, enthalpy, and entropy changes associated with the equilibrium adsorption constant, are computed according to Eq. 17.

$$K_0 = \frac{C_0 - C_e}{C_e} \quad (17)$$

Where C_0 and C_e are the initial and equilibrium concentrations. Gibbs free energy was obtained at different temperatures using Eq. 18 [16].

$$\Delta G^{\circ}_{ads} = -RT \ln K_0 \quad (18)$$

Enthalpy adsorption was obtained of the Van 't Hoff Equation from the slope of $\ln K_0$ curve in term of 1/T, using the following Eq. 19.

$$\ln K_0 = \frac{\Delta S^0}{R} - \frac{\Delta H^0}{RT} \quad (19)$$

Where ΔS^0 is the variation of entropy in terms of J.mol.K^{-1} and T, ΔH^0 and R are in kelvin, J.mol$^{-1,}$ and J.mol^{-1}k$^{-1,}$ respectively. The adsorption thermodynamics constant is presented in Table 9.

Table 9. Thermodynamic parameters for the adsorption of MO dye onto Fe_3O_4@HA/MMT.

Tem. (K)	$\Delta G^0, \frac{kJ}{mol}$	$\Delta S^0, \frac{J}{mol.K}$	$\Delta H^0, \frac{kJ}{mol}$	$E_0, \frac{kJ}{mol}$	S^0
288	-6.259	88.843	+19.314	+18.3	3.04×10^{-5}
298	-7.279				
308	-7.873				
318	-8.980				
328	-9.859				

To investigate the dominant adsorption type in this study, activation energy (E_a) and adhesion probability (S^*) were estimated from experimental data. Activation energy is calculated from Eq. 20, using the modified Arrhenius equation is related to surface coverage.

$$S^* = (1-\theta)e^{-(E_a/RT)} \quad (20)$$

Where θ is surface coverage, and S^* is adhesion probability, whose value is in the range of 0-1, and this value depends on the temperature of the system. S^* indicates the amount of absorbed ability to remain on the adsorbent. Surface coverage can be calculated using Eq. 21 [17].

$$\theta = \left[1 - \frac{C_e}{C_0}\right] \quad (21)$$

From the graph of ln [1- θ] in terms of 1/T, the amount of activation energy was obtained. In Table 9, ΔG^o values were obtained at all negative temperatures. Notably, the amount of ΔG^o to -20 kJ.mol^{-1} is consistent with the electrostatic interaction between adsorption sites and adsorbed molecules (physical adsorption), while ΔG^o has a more negative value than -40 kJ.mol^{-1} indicates the formation of a chemical bond between the adsorbent and the adsorbed molecules (chemical adsorption) [18]. The values of ΔG^o obtained at all studied temperatures are less than -10 kJ.mol^{-1}, indicating the process's physical adsorption. The positive value of $\Delta H°$ indicates that the dye adsorption process is endothermic, which may be attributed to temperature-induced structural changes in the adsorbent, such as the swelling of layers, facilitating greater dye uptake. The results of increasing adsorption are quite consistent with increasing temperature. The positive $\Delta S°$ indicate an increase in irregularity and probability of collisions between methyl orange molecules and the adsorbent surface in the process of dye adsorption. From the slope of the diagram, the activation energy value of 18.3 kJ.mol^{-1} was obtained. The positive activation energy values indicate the endothermic nature of the adsorption process. The value of S* is minimal and close to zero (S* << 1), indicating a high probability of methyl orange molecules adhering to the adsorbent surface and confirming that the process is governed by physical adsorption.

Conclusions

In this study, natural materials-montmorillonite and humic acid were combined with iron oxide to synthesize effective, magnetically responsive adsorbents. Using software-based experimental design, the influence of five parameters on methyl orange dye adsorption was investigated: adsorbent dosage, pH, humic acid weight percentage, montmorillonite weight percentage, and initial dye concentration. Optimal dye removal was achieved with an adsorbent comprising 50% humic acid in the shell surrounding iron oxide and 13.16% montmorillonite, at an adsorbent dosage of 3.58 g/L, pH 3, and an initial methyl orange concentration of 5 ppm. Kinetic analysis revealed that the pseudo-second-order model best described the adsorption process, exhibiting the highest correlation coefficient, indicating that the adsorption kinetics follow a second-order mechanism. Equilibrium data were analyzed using Langmuir, Freundlich, Temkin, Dubinin–Radushkevich (D-R), and

Harkins–Jura (H-J) isotherm models, with adsorption behavior conforming to the Freundlich isotherm, suggesting multilayer adsorption on a heterogeneous surface. Thermodynamic parameters further characterized the adsorption: negative Gibbs free energy (ΔG°) values confirmed the spontaneity and physical nature of the adsorption; positive enthalpy change (ΔH°) indicated an endothermic process; and a positive entropy change (ΔS°) reflected increased randomness and enhanced interaction probability between dye molecules and the adsorbent surface. The positive activation energy (Ea) corroborated the endothermic adsorption mechanism, while a minimal sticking probability (S* near zero) reinforced the predominance of physical adsorption. These findings demonstrate that montmorillonite and humic acid, when integrated with iron oxide, form a highly efficient, magnetically separable adsorbent suitable for effective methyl orange dye removal under optimized conditions

References

[1]. Choy, J.-H., Clay minerals and layered double hydroxides for novel biological applications, ***Applied Clay Science***, **2007**, 36, 122-132. https://doi.org/10.1016/j.clay.2006.07.007

[2]. Feng, J., Shi, Z., Shan, X., Xing, B., Coating Fe3O4 magnetic nanoparticles with humic acid for high efficient removal of heavy metals in water, ***Environmental Science & Technology***, **2008**, 42, 6949–6954. https://doi.org/10.1021/es800924c

[3]. Haijiao, H., Jie, L., Fan, W., Hongbo, X., Tao, B., Heng, H., Highly efficient and reusable montmorillonite/Fe3O4/humic acid nanocomposites for simultaneous removal of Cr(VI) and aniline, ***Nanomaterials***, **2018**, 8, 976. https://doi.org/10.3390/nano8070537

[4]. Nasrin, N., Hosseini, A., Zohdi, Y., Ghasemi, B., Photocatalytic removal of reactive red 198 from aqueous solution using titanium dioxide photocatalyst supported on Fe-ZSM-5 zeolite, ***Journal of Mazandaran University of Medical Sciences,*** **2017**, 27, 1. https://doi.org/10.1108/PRT-05-2022 0067?urlappend=%3Futm_source%3Dresearchgate

[5]. Nam, S., Han, H., Kang, M. G., Choi, H., Kang, J. H., Photocatalytic Degradation of Acesulfame K: Optimization Using the Box-Behnken Design (BBD), ***Process Safety and Environment Protection***, **2017**, 113, 0305-1. https://doi.org/10.1016/j.psep.2017.09.002

[6]. Lagergren, S., Zur Theorie der Sogenannten Adsorption Gelöster Stoffe, ***Kungliga Svenska Vetenskapsakademiens Handlingar***, **1898**, 24, 1–39. https://doi.org/10.1007/BF01501332

[7]. Yang, X., Al-Duri, B., Kinetic modeling of liquid-phase adsorption of reactive dyes on activated carbon, ***Journal of Colloid and Interface Science***, **2005**, 287, 25–34. https://doi.org/10.1016/j.jcis.2005.01.093

[8]. Azizian, S., A new empirical rate equation for adsorption kinetics at solid/solution interface, ***Applied Surface Science***, **2010**, 256, 5153–5156. https://doi.org/10.1016/j.apsusc.2009.12.080

[9]. Ho, Y. S., McKay, G., Pseudo-second order model for sorption processes, ***Process Biochemistry***, **1999**, 34, 451–465. https://doi.org/10.1016/S0032-9592(98)00112-5

[10]. Chien, S. H., Clayton, W. R., Application of Elovich equation to the kinetics of phosphate release and sorption in soils, ***Soil Science Society of America Journal***, **1980**, 44, 265–268. https://doi.org/10.2136/sssaj1980.03615995004400020013x

[11]. Weber, W. J., Morris, J. C., Kinetics of adsorption on carbon from solution, ***Journal of the Sanitary Engineering Division***, **1963**, 89, 31–59. https://doi.org/10.1061/JSEDAI.0000430

[12]. Abdelwahab, O., Evaluation of the use of loofa activated carbons as potential adsorbents for aqueous solutions containing dye, ***Desalination***, **2008**, 222, 357–367. https://doi.org/10.1016/j.desal.2007.01.146

[13]. Freundlich, H. M. F., Over the adsorption in solution, ***The Journal of Physical Chemistry***, **1906**, 57, 385–471. DOI: 10.12691/aees-9-10-2

[14]. Temkin, M. I., Pyzhev, V., Kinetics of ammonia synthesis on promoted iron catalysts, ***Acta Physicochimica URSS***, **1940**, 12, 217–222. DOI: 10.12691/ijebb-4-2-4

[15]. Dubinin, M. M., Radushkevich, L. V., The equation of the characteristic curve of activated charcoal, ***Proceedings of the Academy of Sciences of the USSR, Physical Chemistry Section***, **1947**, 55, 331-337.

[16]. Basar, C. A., Applicability of the various adsorption models of three dyes adsorption onto activated carbon prepared waste apricot, ***Journal of Hazardous Materials***, **2006**, 135, 232–241. DOI: 10.1016/j.jhazmat.2005.11.055

[17]. Kannan, N., Sundaram, M. M., Kinetics and mechanism of removal of methylene blue by adsorption on various carbons—a comparative study, **Dyes and Pigments**, **2001**, 51, 25–40. DOI: 10.1016/S0143-7208(01)00028-0

[18]. Jnr, M. H., Spiff, A. A., Effect of temperature on the sorption of Pb2+ and Cd2+ from aqueous solution by Caladium bicolor (wild cocoyam) biomass, Electronic ***Journal of Biotechnology***, **2005**, 8, 162–169. DOI: 10.2225/vol8-issue2-fulltext-8

[19]. Rieman, W., Walton, H. F., Ion Exchange in Analytical Chemistry, International Series of Monographs in Analytical Chemistry, ***Pergamon Press***, **1970**.

[20]. El-Khaiary, M. I., Kinetics and mechanism of adsorption of methylene blue from aqueous solution by nitric acid treated water-hyacinth, ***Journal of Hazardous Materials***, **2007**, 147, 28–36. DOI: 10.1016/j.jhazmat.2007.01.122

[21]. Pehlivan, E., Baybara, A., Tuna, K., Parlayıcı, S., Utilization of eco-friendly gelatin for Cr(VI) adsorption, **Desalination and Water Treatment**, **2017**, 81, 308–315. DOI: 10.5004/dwt.2017.20876

[22]. Chen, C., Geng, X., Huang, W., Adsorption of 4-chlorophenol and aniline by nanosized activated carbons, **Chemical Engineering Journal**, **2017**, 327, 941–952. DOI: 10.1016/j.cej.2017.06.074

[23]. Ontañon, O., González, P., Barros, G., Agostini, E., Improvement of simultaneous Cr (VI) and phenol removal by an immobilised bacterial consortium and characterisation of biodegradation products, **New Biotechnology**, **2017**, 37, 172–179. DOI: 10.1016/j.nbt.2016.12.003

[24]. Li, X., Jin, X., Zhao, N., Angelidaki, I., Zhang, Y., Efficient treatment of aniline containing wastewater in bipolar membrane microbial electrolysis cell-Fenton system, **Water Research, 2017**, 119, 67–72. DOI: 10.1016/j.watres.2017.04.046

[25]. Xie, Q., Zhou, H., Lv, Z., Liu, H., Guo, H., Sn4+ self-doped hollow cubic SnS as an efficient visible-light photocatalyst for Cr (VI) reduction and detoxification of cyanide, **Journal of Materials Chemistry A**, **2017**, 5, 6299–6309. DOI: 10.1039/C6TA10253C

[26]. Pirsaheb, M., Shahmoradi, B., Beikmohammadi, M., Azizi, E., Hossini, H., Photocatalytic degradation of Aniline from aqueous solutions under sunlight illumination using immobilized Cr: ZnO nanoparticles, **Scientific Reports**, **2017**, 7, 1473. DOI: 10.1038/s41598-017-01429-5

[27]. Pérez-Prior, M., Gómez-Bombarelli, R., González-Sánchez, M., Valero, E., Biocatalytic oxidation of phenolic compounds by bovine methemoglobin in the presence of H2O2: Quantitative structure–activity relationships, ***Journal of Hazardous Materials***, **2012**, 217-218, 207–215. DOI: 10.1016/j.jhazmat.2012.02.004

[28]. Valero, E., Pérez-Prior, M., González-Sánchez, M., Removal of aromatic compounds from wastewater by hemoglobin soluble and immobilized on Eupergit® CM, ***Environmental Engineering and Management Journal*, 2014**, 13, 2459–2466. DOI: 10.30638/eemj.2014.274

[29]. Kalantari, K., Ahmad, M., Shameli, K., Hussein, B., Khandanlou, R., Khanehzaei, H., Size-Controlled synthesis of Fe3O4 magnetic nanoparticles in the layers of montmorillonite, ***Journal of Nanomaterials***, **2014**, 2014, 181. https://doi.org/10.1155/2014/739485

[30]. Illés, E., Tombácz, E., The effect of humic acid adsorption on pH-dependent surface charging and aggregation of magnetite nanoparticles, ***Journal of Colloid and Interface Science***, **2006**, 295, 115–123. https://doi.org/10.1016/j.jcis.2005.08.003